

Jui-Ting Lee,¹ Kai-Cheng Tien,² Yen Te Ho,³ and An-Bin Huang⁴

A Fiber Optic Sensored Triaxial Testing Device

ABSTRACT: The physical quantities involved in a triaxial testing device have mostly been monitored with electric sensors. These sensors are currently subject to short circuit when submerged under water and electromagnetic interference (EMI). Waterproofing and EMI noise filtration have often been a challenge to the triaxial test set-up. These drawbacks can be substantially minimized when using optic fiber sensors. The optic fiber Bragg grating (FBG) sensors have the additional advantage of being partially distributive where multiple sensors can share the same signal transmission line. Taking advantage of these unique capabilities, the authors explored the possibility of converting all pressure/force and linear displacement transducers in a triaxial testing device into FBG based sensors. A series of shearing tests on unsaturated and saturated soil specimens were carried out using the new FBG sensored triaxial testing device. In most cases, the measurement of physical quantities was paired with electric sensors so that the results can be compared. This paper describes the principles of the individual FBG sensor designs and demonstrates their applications in triaxial testing.

KEYWORDS: fiber Bragg grating, triaxial test, unsaturated soil, sand

Introduction

The instrumentation involved in triaxial shearing tests can include measurements of force, displacement, and pressure. Highly sensitive electric devices coupled with an automated data logging system are often used in modern-day triaxial testing set-ups. To minimize system errors, it has been advocated that some of the measurements be made locally (Burland 1989) from inside of the triaxial cell. Under these circumstances the sensors are likely to be submerged under water. The electric sensors are subject to electromagnetic interference (EMI), prone to zero shift and short circuit when exposed in water for a prolonged period. Waterproofing and EMI noise filtration have always been a challenge in setting up these electric sensors for triaxial tests.

The optic fiber sensors typically transmit signals via light and thus are not affected by EMI. Unless electric circuits are involved, the optic fiber sensors can be submerged under water without the concern of short circuit. The authors have developed a number of optic fiber sensors originally for monitoring stability of earth slopes. These monitoring devices used the optic fiber Bragg grating (FBG) as the key sensing element. New developments included FBG segmented deflectometer (FBG-SD) for ground displacement monitoring (Ho et al. 2006) and FBG pressure transducers for measuring pore water pressures (Ho et al. 2008). In addition to the advantages of the optic fiber sensors as stated above, the FBG is partially distributive where multiple FBG sensors can share the same optic fiber for signal transmission. The FBG sensors are passive in nature where a return signal is generated only when provoked by an external light source. No electric circuit is buried under ground

with the sensors when installed in the field. These features are rather desirable in enhancing the efficiency, durability, and stability of the sensors when deployed in the field for geotechnical instrumentation applications.

The aim of this paper is to explore and demonstrate the unique capabilities of the fully FBG based sensors when used in a triaxial testing device. By making necessary modifications from the above described field monitoring devices, a series of FBG based sensors suitable for triaxial testing were developed. These sensors include a force transducer, linear displacement sensor, and a series of gauge/differential pressure transducers. The triaxial testing device can be configured to perform tests on unsaturated soil specimens with matric suction and specimen volume change measurements. The testing device can also be fitted to conduct conventional triaxial tests on saturated soil specimens with pore pressure (undrained) or specimen volume change (drained) measurements. A series of triaxial tests on unsaturated silty sand from Yu Feng, Taiwan and on saturated clean sand from Da Nang, Vietnam were conducted using the new testing system. In most cases, the FBG sensors were coupled with a conventional electric transducer where the measurements can be compared for evaluation of consistency. This paper introduces the basic principle of FBG, design, and calibration of the various FBG sensors developed for triaxial testing. The effectiveness of the FBG sensored triaxial test device is evaluated based on the available test results.

FBG as a Partially Distributive Strain Sensor

Optical fibers are made of silica, with a diameter about the same of a human hair, and can transmit light over large distances with very little loss. Optical fibers comprise two essential components: A core surrounded by an annular cladding. The core of the optical fiber serves to guide light along the length of the optical fiber. The cladding has a slightly lower index of refraction than the core. Its primary function is to ensure total internal reflection within the core and that very little light is lost as it propagates along the core of the optical fiber. These important properties lie at the heart of the fiber optic telecommunication industry. The typical combined di-

Manuscript received November 1, 2009; accepted for publication November 19, 2010; published online December 2010.

¹Dept. of Civil Engineering, National Chiao-Tung Univ., Hsinchu, Taiwan, e-mail: ruiting.cv92g@nctu.edu.tw

²G.T. International, Nanjing S. Rd., Section 3, No. 215, 2F, Taipei, Taiwan, e-mail: gti.taipei@msa.hinet.net

³Dept. of Civil Engineering, National Chiao-Tung Univ., Hsinchu, Taiwan, e-mail: ytho.2004@seed.net.tw

⁴Professor, Department of Civil Engineering, National Chiao-Tung Univ., Hsinchu, Taiwan (Corresponding author), e-mail: abhuang@mail.nctu.edu.tw

iameter of core and cladding is 125 μm . The silica core/cladding is protected by an acrylic coating. The total outside diameter of an optical fiber with the acrylic coating is 250 μm . There are other types of optical fibers of different dimensions and materials for various purposes. Readers are referred to Agrawal (2002) for more details on fiber optic communication systems. By adopting technologies from telecommunication systems, many fiber optic based sensing techniques have been developed in the past few decades. These sensors have been used in medical, defense, aeronautical, and civil engineering industries. Development and application of fiber optic sensors are expanding rapidly as indicated by the well-attended conferences organized by many international societies such as the International Society for Optical Engineering (SPIE). The related conference proceedings are readily available through SPIE. The fiber optic Bragg grating (FBG) is one of the many available forms of optical fiber sensors. An FBG is formed when a periodic variation of the index of refraction is created along a section of an optical fiber. The formation of permanent grating in an optical fiber was first demonstrated by Hill et al. (1978). Following this concept, Meltz et al. (1989) pioneered the techniques of producing in-FBG strain sensors. A periodic variation or modulation of fiber core refractive index is formed by exposing that 1 to 20 mm segment of single mode optic fiber to a spatial pattern of ultraviolet light. When the FBG is illuminated by a wideband light source, a fraction of the light is reflected back upon interference by the FBG. The wavelength of the reflected light, or the Bragg wavelength, λ_B is related to the period of the index modulation, Λ , and effective fiber core index of refractive, n , as expressed by (Rao 1998)

$$\lambda_B = 2n\Lambda \quad (1)$$

Longitudinal strains within the Bragg grating, ε_B , induced by variations in temperature or stress can cause a change in Λ and thus a shifting of λ_B , with the following approximate relationships (Rao 1998):

$$\Delta\lambda_B = 0.74\lambda_B\varepsilon_B \quad (2)$$

and

$$\Delta\lambda_B = 8.9 \times 10^{-6}\lambda_B\Delta C^\circ \quad (3)$$

where:

ΔC° =change of temperature in degree Celsius.

The constants in Eqs 2 and 3 can vary, depending on the photoelastic properties of the optic fiber. For the FBG sensors reported herein, the λ_B ranged from 1520 to 1570 nm (10^{-9} m). A typical

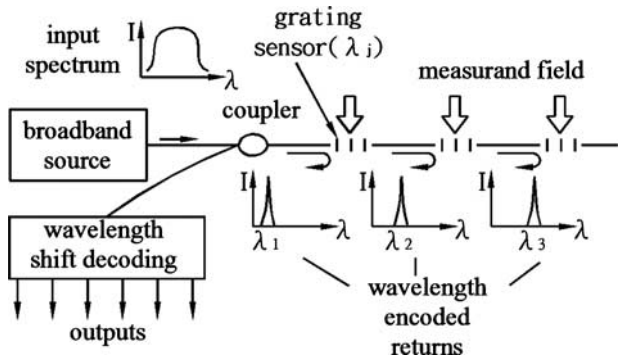


FIG. 1—Schematic diagram of FBG (after Kersey 1992).

commercially available FBG data acquisition system can detect a shifting of λ_B as small as 1 picometer (pm) ($\text{pm}=10^{-12}$ m), which corresponds to a strain (ε_B) of the order of 10^{-6} according to Eq 2. This is well above desirable resolution for strain sensors. In addition, the strain ε_B is determined through the change of λ_B which is relatively immune to variations in the strength of light source. This unique feature makes FBG less likely to have signal drifting.

The returned signal from every FBG carries a unique range or domain of wavelength $\lambda_B + \Delta\lambda_B$, making it possible to have multiple FBG elements on the same fiber. The multiplexing among various sensors on a single fiber can be accomplished by wavelength division addressing as conceptually described in Fig. 1. Most of the silica optical fiber breaks at a strain of 0.1 % (10^{-3}) which corresponds to a $\Delta\lambda_B$ of approximately 10 nm. Thus, a separation of λ_B in 2–3 nm between FBGs would be sufficient in most cases. The FBG is partially distributive because only those parts of the optic fiber with FBG are used as strain sensors and these sensors can share the same optic fiber transmission line. In contrast, the conventional electric resistance strain gauge is non-distributive. A set of wires is dedicated to a specific strain gauge.

With proper configuration, all advantages of the FBG stated above can be inherited in FBG-based transducers. These advantages can include: Capability of being partially distributive, high resolution, good signal stability, and immune to EMI. The authors have developed a few devices using FBGs. These developments included an FBG-SD for ground displacement monitoring (Ho et al. 2006) and FBG pressure transducers for measuring pore water pressures (Ho et al. 2008). Following similar principles, the authors developed a series of displacement, pressure, and force measure-

TABLE 1—FBG based sensors made for triaxial testing device.

Sensor description	Specifications	Origin of Design Concept
Linear displacement transducer	Full range: 20 mm Sensitivity: 3.7 μm Accuracy: ± 1.16 % full scale	Ho et al. (2006)
Load cell	Full range: 1 kN Sensitivity: 1 N Accuracy: ± 0.493 % full scale	Ho et al. (2008)
Gauge pressure transducer	Full range: 500 kPa Sensitivity: 0.08 kPa Accuracy: ± 0.434 % full scale	Ho et al. (2008)
Differential pressure transducer	Full range: 50 mm water head Sensitivity: 0.36 mm water head Accuracy: ± 1.35 % full scale	Ho et al. (2008)

Note: Accuracy = $\sqrt{\sum(\text{measured value} - \text{calibration curve})^2 / (\text{number of measurements} - 1)}$.

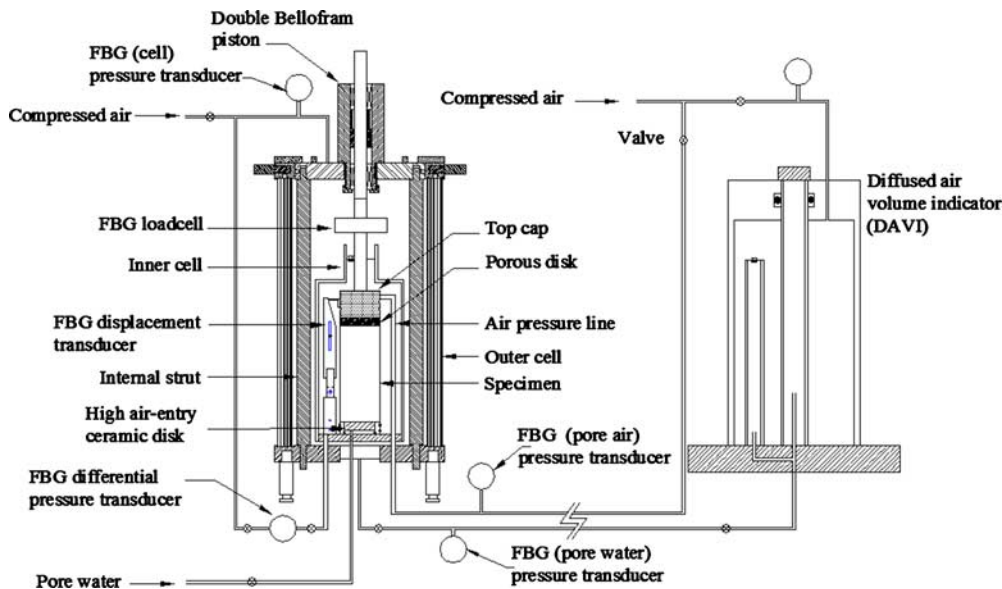


FIG. 2—Schematic view of the testing system.

ment transducers for triaxial testing. Table 1 summarizes the transducers specifically made for a triaxial testing device and their relationship in design principles with the field monitoring devices developed earlier by the authors.

The triaxial testing device as schematically shown in Fig. 2 was set up for tests on unsaturated soil specimens. The system involved three FBG gauge pressure transducers and one for each of the rest of the transducers included in Table 1. The gauge pressure transducers were used to measure the cell, pore-air, and pore water pressure, respectively. The pedestal was fitted with a high air entry ceramic to facilitate matric suction measurement. The volume change of the unsaturated soil specimen during shearing was monitored using a double cell design (Ng et al. 2002). Fluctuation of the water level within the inner cell caused by the specimen volume change was monitored using the FBG differential pressure transducer. The linear displacement transducer and load cell were both mounted inside of the triaxial cell for internal measurements. An isolated FBG was used as a temperature sensor to monitor the fluctuation of temperature during triaxial test. By removing the inner cell and replacing the high air entry ceramic with a conventional porous stone at the pedestal, the triaxial testing system can be used to conduct drained or undrained shearing tests on saturated specimens with pore water pressure or volume change monitoring. Details of the design principles of the transducers for triaxial testing are described in the following sections.

The FBG Displacement Transducer

A schematic view of the displacement transducer is shown in Fig. 3. The displacement transducer is fixed to the base of the inner cell. A bracket is fixed to the top cap. The bracket pushes against an inclined plane of the displacement transducer. The contact point at the bracket and the surface of the inclined plane of the displacement transducer were carefully polished to minimize friction. The angle of inclination is 75° from horizontal direction. A downward linear displacement of the bracket $\Delta\delta$ causes the top part of the displacement transducer to rotate by an angle θ against the hinge. For an initial distance from hinge to the contact point between

bracket and inclined plane L , the relationship between $\Delta\delta$ (in millimeters) is related to θ (in degree) as

$$\Delta\delta = \frac{L[\sin \theta \times \tan 75^\circ - (1 - \cos \theta)]}{(\cos \theta + \sin \theta \times \tan 75^\circ)} \quad (4)$$

The relationship between $\Delta\delta$ and θ is non-linear and dependent on L . Rotation between the bottom and top part of the displacement transducer causes deflection of a flexible rod placed within the transducer. The lower end of the flexible rod is fixed to the bottom part of the displacement transducer. The upper end is supported by a pin that is free to slide and rotate in a slot. Principles of the deflection measurement using the two-segment design can be found in Ho et al. (2006). A pair of FBGs are fixed to the opposite sides of

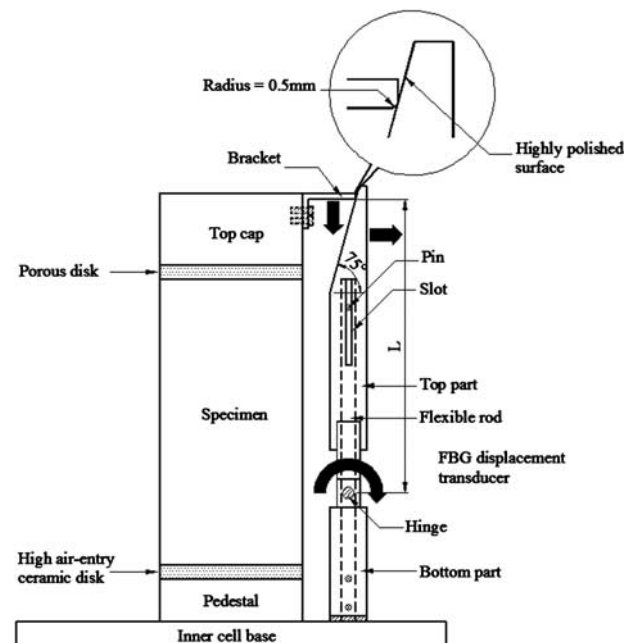


FIG. 3—The FBG displacement transducer.

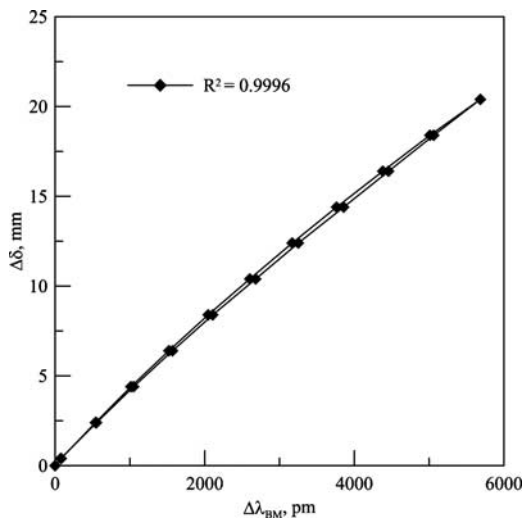


FIG. 4—Calibration result of the FBG displacement transducer.

the flexible rod to measure the flexural strains as a result of deflection. To take into consideration of temperature effects, the change in wavelengths from these two FBGs (i.e., $\Delta\lambda_{B1}$ and $\Delta\lambda_{B2}$) are subtracted and averaged to obtain the measured value $\Delta\lambda_{BM}$ as

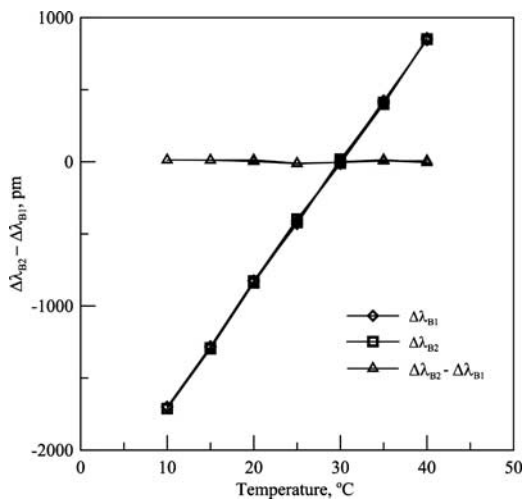


FIG. 5—Correction of temperature effects for FBG displacement transducer.

$$\Delta\lambda_{BM} = \frac{1}{2}(\Delta\lambda_{B1} - \Delta\lambda_{B2}) \quad (5)$$

The amount of deflection θ is measured through $\Delta\lambda_{BM}$ and there is a linear θ - $\Delta\lambda_{BM}$ relationship (Ho et al. 2006). According to this θ - $\Delta\lambda_{BM}$ relationship and Eq 4, $\Delta\delta$ can be determined by $\Delta\lambda_{BM}$ measurements. Figure 4 shows the relationship between $\Delta\lambda_{BM}$ and $\Delta\delta$ from calibrations by setting $L=100$ mm. The maximum displacement of 20 mm corresponds to $\Delta\lambda_{BM}$ of 5400 pm. The FBG acquisition unit has a resolution of 1 pm. Thus the displacement transducer has a resolution of 3.7 μm .

The effectiveness of nullifying the temperature is demonstrated in Fig. 5. The displacement transducer was placed inside a thermal chamber where the temperature fluctuated from 10°–40°C. The corresponding readings of $\Delta\lambda_{B1}$ and $\Delta\lambda_{B2}$ changed from -1700 to 950 pm. The $\Delta\lambda_{BM}$ however, remains within a range of ± 5 pm. In the triaxial tests to be described later, the air conditioned room temperature was set at 25°C. Temperature fluctuation during triaxial shearing did not exceed ± 1.5 °C, much less than the 30°C range applied in the calibration. The potential error after correction for temperature fluctuation is thus expected to be rather insignificant.

The FBG Load Cell

The design of FBG load cell follows the concept of a donut load cell. The force to be measured is applied at the center of a circular diaphragm with a clamped edge as schematically shown in Fig. 6. The 0.3 mm thick stainless steel diaphragm had a diameter of 65 mm. The original design had a pair of FBGs attached towards the edge of the diaphragm in the radial direction, on the opposite sides of the diaphragm. A concentrated load applied at the center would cause these two FBGs experience strains in equal magnitude but opposite signs according to theory of plates and shells (Timoshenko and Woinowsky-Krieger 1959). Taking advantage of these characteristics and invoking Eq 5, the temperature compensated $\Delta\lambda_{BM}$ from the two FBG readings are used to modulate the applied load. The compression tests on unsaturated Yu Feng sand used the original load cell design.

It was concerned that off-centered or inclined force applied to the load cell with one pair of FBGs could result in reading errors. Two additional pairs of FBGs were added to the load cell. These FBG pairs were distributed at 120° apart as shown in Fig. 6. The axial load experienced by the load cell was determined based on the average of the three pairs of the FBGs. Figure 7 shows the calibra-

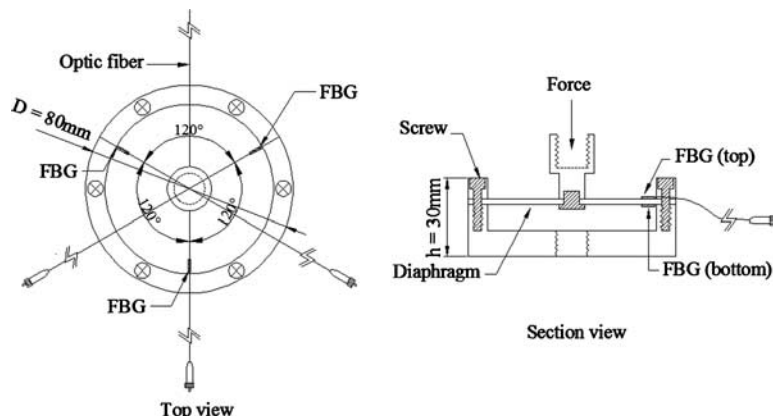


FIG. 6—Schematic views of a FBG load cell.

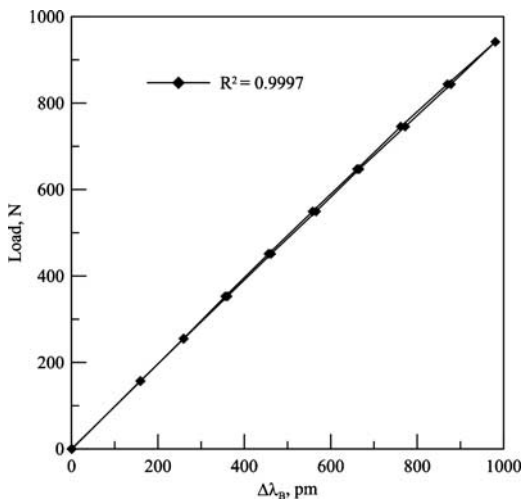


FIG. 7—Calibration result of the FBG load cell.

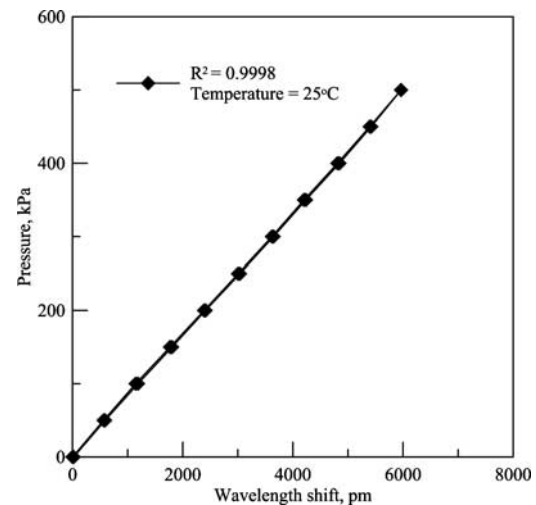


FIG. 9—Calibration result of a gauge FBG pressure transducer.

tion results of this modified 1 kN load cell. The 1 kN applied load corresponds to a reading of 1000 pm. Considering an FBG acquisition system capable of detecting $\Delta\lambda_B$ at 1 pm, the load cell has a resolution of approximately 1 N. Compression tests on saturated Da Nang sand used the modified load cell with three pairs of FBGs.

The FBG Gauge Pressure/Differential Pressure Transducer

The same design principles of the load cell as described above can also be used for a pressure transducer. In this case, one side of the diaphragm is sealed to form an air-tight chamber and no concentrated force is applied. The FBGs can be used to sensor the straining of the diaphragm in response to changes in pressure (Ho et al. 2008). This design however, lacks desirable sensitivity unless a rather large diaphragm is used. An alternative design as shown in Fig. 8 was used for pressure transducers. The design also involves a circular diaphragm clamped on the edge. An FBG was used to measure the deflection of the diaphragm at its center as a result of pressure changes.

The diaphragm separates the reference and input pressure chambers. The optic fiber that contains an FBG pierced through the center of the diaphragm was epoxied at both ends to the body of the pressure transducer and piercing point, in order to fix the position of the optic fiber and seal off the two chambers. When used as a gauge pressure transducer, the reference chamber can be exposed to the atmospheric pressure. The reference chamber is connected to

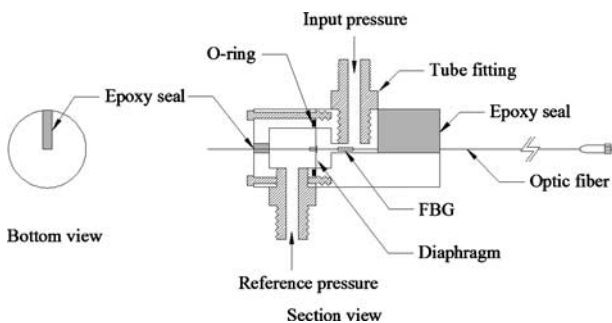


FIG. 8—Schematic views of a FBG pressure transducer.

a controlled reference pressure when used as a differential pressure transducer. The amount of deflection at center of the diaphragm is linearly related to the pressure difference between the reference and input pressure chambers (Timoshenko and Woinowsky-Krieger 1959). Sensitivity and range of the pressure transducer can be adjusted by changing the thickness and diameter of the diaphragm.

A disadvantage of the single FBG design is that the temperature effects are not compensated. A scheme that involves independent temperature sensing and reading adjustment was used to compensate the effects of temperature fluctuations. The pressure transducer was placed inside of a thermal chamber first to calibrate the effects of temperature fluctuations on the FBG readings when the transducer was subject to a constantly applied pressure. The results provide a relationship between temperature and wavelength change caused by temperature fluctuation $\Delta\lambda_{BT}$ (i.e., $\Delta\lambda_{BT}$ —temperature relationship). With the temperature and thus $\Delta\lambda_{BT}$ known, a corrected wavelength change $\Delta\lambda_{Bc}$ is obtained from the original FBG measurement $\Delta\lambda_{Bm}$ by

$$\Delta\lambda_{Bc} = \Delta\lambda_{Bm} \pm \Delta\lambda_{BT} \quad (6)$$

An FBG sealed inside of a stainless steel tube, placed alongside with the pressure transducers was used as a temperature sensor. A relationship between temperature and readings from the temperature sensor FBG, $\Delta\lambda_{Bts}$ is obtained by calibrating the sensor inside a thermal chamber. Figure 9 shows the calibration results of a gauge pressure transducer performed in a thermal chamber under a controlled temperature of 25°C. The stainless steel diaphragm was 13 mm in diameter and 0.2 mm thick. The material was typically used to make spring coil with very elastic behavior. For a full range of 500 kPa, the gauge pressure transducer had a resolution of 0.08 kPa. The same design was used for all the gauge pressure transducers reported herein. Figure 10 depicts the calibration result of the differential pressure transducer under a controlled temperature of 25°C. The differential pressure transducer used a 40 mm diameter and 0.2 mm thick diaphragm. With a full range of 50 mm water head, results show a resolution of 0.36 mm of water head.

Results from the calibrations of the FBG temperature sensor and a gauge pressure transducer are shown in Fig. 11. The gauge pressure transducer was calibrated by applying a constant pressure to the transducer while imposing temperature fluctuation in a thermal chamber. For the range of temperature and pressure applied, the

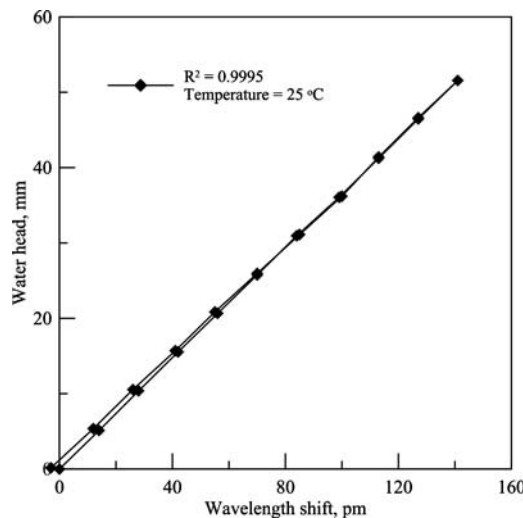


FIG. 10—Calibration result of a differential FBG pressure transducer.

relationship between $\Delta\lambda_{BT}$ and temperature was not significantly affected by pressure. Thus, a single $\Delta\lambda_{BT}$ –temperature relationship was used when correcting the FBG readings to obtain $\Delta\lambda_{Bc}$ from Eq 6. The effectiveness in temperature correction scheme is demonstrated in Fig. 12. A gauge pressure transducer was subjected to a constant pressure and placed inside a thermal camber where temperature changed from 10 to 40 °C. For the pressures and range of temperatures applied, the fluctuation of $\Delta\lambda_{Bm}$ by as much as ± 250 pm, the fluctuation of $\Delta\lambda_{Bc}$ was reduced to no more than 2 pm

Triaxial Test Results

The triaxial cell equipped with a double Bellofram piston, used for the experiment was originally manufactured by Seiken Inc. of Japan. A 3Bar high air entry ceramic porous stone was fitted to the pedestal to facilitate unsaturated soil triaxial tests, taking advantage of the axis-translation technique. A photograph of the triaxial cell with the FBG sensors is depicted in Fig. 13. An external electric load cell, electric linear variable displacement transducer and two electric pressure transducers (for pore water and pore air pressure

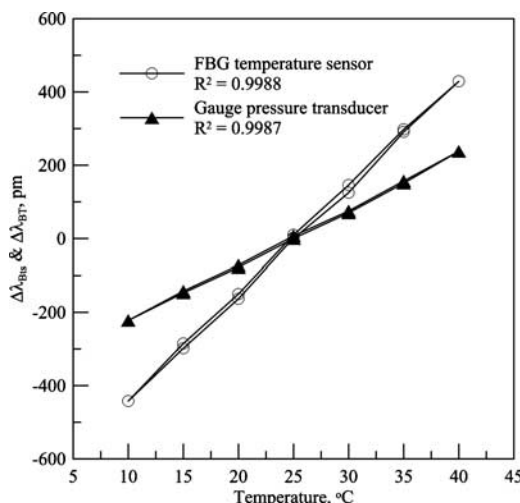


FIG. 11—Calibration for temperature effects on FBG pressure transducer.

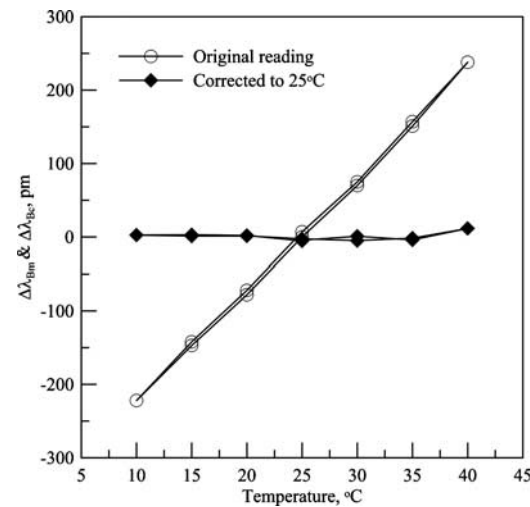


FIG. 12—Correction of temperature effects for FBG pressure transducer.

measurements) were installed to provide reference readings for comparison purposes. The electric and FBG pressure transducers were connected to the same respective drainage lines.

Compression Tests on Unsaturated Yu Feng Sand

Soil sample taken from Yu Feng, a village in the catch basin of Shi-Men reservoir in northern Taiwan was used for this series of shearing test. Figure 14 shows the grain size distribution of Yu Feng sand. The non-plastic silty sand with 9 % of fines (particles passing #200 sieve) had a specific gravity (G_s) of 2.68. The soil sample taken from the field was oven dried, pulverized, and then mixed with 8 % of water content to reconstitute the 50 mm diameter and 100 mm height soil specimen in five layers, following a wet tamping procedure. The specimen was then saturated in the triaxial cell under a back pressure of 200 kPa. Upon saturation and B check, the pore-air pressure (u_a) was raised against the 200 kPa water back pressure to reach the desired difference between u_a and pore-water

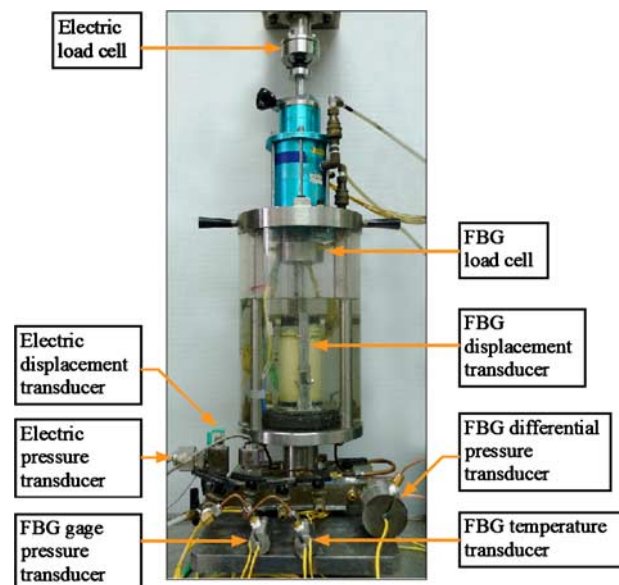
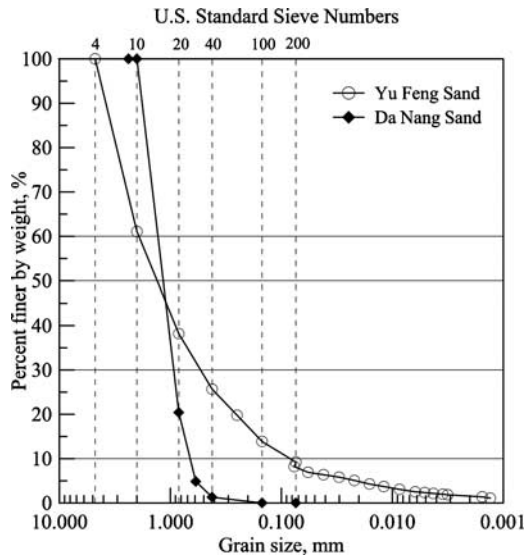


FIG. 13—The fiber optic sensored triaxial cell.

FIG. 14—*Grain size distribution of the tested soils.*

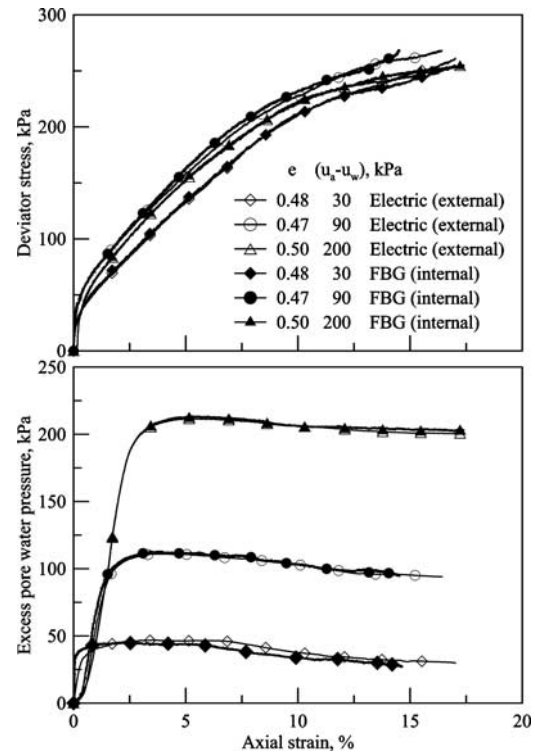
pressure (u_w), i.e., the matric suction ($u_a - u_w$). The cell pressure (σ_c) was raised concurrently with the u_a adjustment to reach and maintain a $(\sigma_c - u_a)$ of 100 kPa. The specimen was then allowed to drain from the bottom of the specimen and consolidate in an unsaturated state.

The shearing by axial compression began when no significant drainage from the specimen could be detected. The unsaturated soil specimen was sheared using a constant water content (CW) method (Fredlund and Rahardjo 1993). In the CW method σ_c and u_a were kept constant, while the pore-water line was closed and u_w was allowed to fluctuate. The axial compression was applied following a constant deformation rate of 0.01 mm per minute. The FBG and electric sensor readings were recorded at 1 Hz frequency. For the results to be presented, the soil specimens had initial $(u_a - u_w)$ values of 30, 90, and 200 kPa. All specimens were compacted to an initial void ratio of approximately 0.5, consolidated and sheared under $(\sigma_c - u_a)$ of 100 kPa.

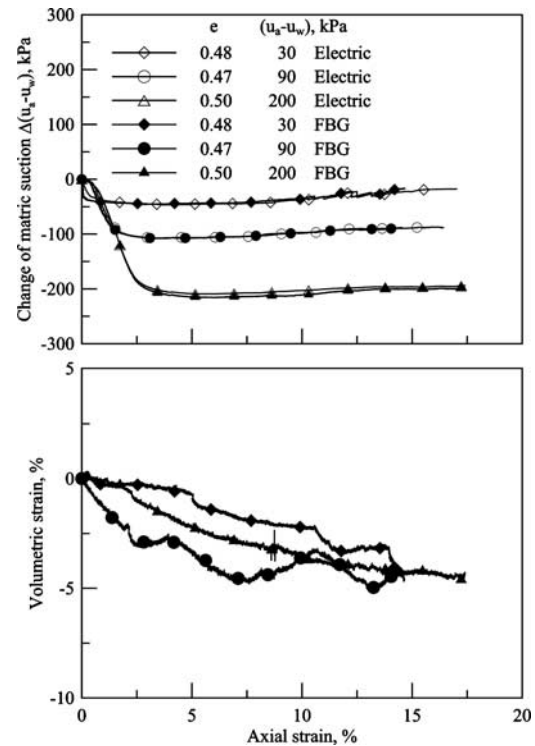
Figure 15 shows the deviator stress, excess pore-water pressure, and axial strain relationships from the series of triaxial tests. Results from the FBG sensors are compared with those from the corresponding electrical sensors. The excess pore-water pressure and axial stress readings are very similar between the FBG and electrical sensors. The matric suction change included in Fig. 16 is a direct derivation of excess pore-water pressure of Fig. 15. The results also demonstrated consistency between the FBG and electric sensors. The volumetric strain readings in Fig. 16 were determined from the inner cell water fluctuation according to FBG differential pressure transducer. All specimens showed a maximum of 4 to 5 % of volumetric contraction according to this series of tests. These volumetric strains correspond to a maximum of 45 mm fluctuation of water level within the inner triaxial cell. This is well within the capability of the FBG differential pressure transducer with a resolution of 0.36 mm.

Compression Tests on Saturated Da Nang Sand

The clean, uniformly graded Da Nang sand was a silica sand imported from Vietnam. The sand was washed, sieved, and oven dried before shipping to the laboratory. The grain size distribution of Da

FIG. 15—*Deviator stress-axial strain and pore water pressure-axial strain relationships from constant water content triaxial tests on Yu Feng Sand.*

Nang sand is included in Fig. 14. The specific gravity G_s was 2.61. The minimum void ratio e_{\min} was 0.515, and the maximum void ratio e_{\max} was 0.808. More details on Da Nang sand can be found in Huang and Hsu (2005).

FIG. 16—*Suction-axial strain and volumetric strain-axial strain relationships from constant water content triaxial tests on Yu Feng Sand.*

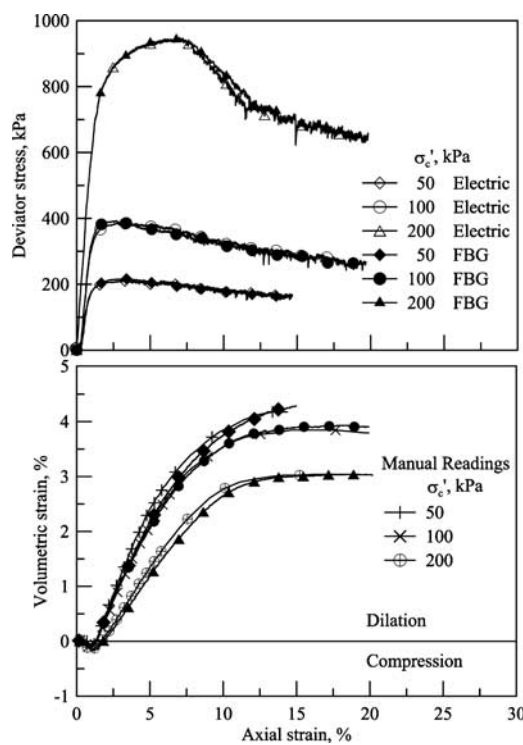


FIG. 17—Deviator stress-axial strain and volumetric strain-axial strain relationships from triaxial tests on Da Nang Sand.

For this series of tests, the high air entry ceramic at the pedestal was replaced with a conventional high permeability porous stone. The inner cell was removed. The load cell was modified by adding two additional pairs of FBGs. The sand specimen with void ratio of 0.66 (relative density=50 %) was prepared by dry pluviation. The specimen was saturated under a back pressure of 300 kPa and consolidated isotropically. A drained axial compression test was conducted upon consolidation, under a constant effective confining stress (σ'_c) and an axial strain rate of 0.1 %/minute. The fluctuation of water level in the pore water burette was monitored using the FBG differential pressure transducer as a means to measure specimen volume change during shearing. The water level in the pore water burette was also recorded manually to provide reference volume change readings for comparison purpose. The sand was dilatant under the test conditions. Figure 17 indicates that all three tests showed consistency between the FBG and reference readings in axial strain, deviator stress and volumetric strain measurements. Most significant differences occurred between the FBG and manual volumetric strain readings. In this case the difference was less than 5 %. The axial strain-deviator stress curves of Fig. 17 showed significant fluctuations in the post-peak region in both the FBG and

electric sensor readings. The fluctuation is likely a reflection of the coarse sand characteristics rather than sensor signal noise.

Observations of the FBG Sensor Performance

The available triaxial test results show that the FBG based sensors can at least provide comparable measurements as their electric counterparts in quality and quantity. The fact that FBG sensors are immune to EMI and short circuit in water made the mechanical design and installation within the triaxial cell relatively easy. An obvious example is the internal FBG load cell. There was no need to make the load cell hermetic and there was no need of liquid infill to offset the triaxial cell pressure. The gauge pressure and differential pressure transducers share the same design principles. Different purposes can be served by changing the diameter and/or thickness of the diaphragm. The FBG displacement transducer shown in Fig. 3 was approximately 190 mm high and 15 mm wide. The design was bulky. Instead of reducing the sizes, it is possible to adopt the local displacement transducer (LDT) developed by Goto et al. (1991). By replacing the four strain gauges attached to the metal strip with a pair of FBGs, the LDT can maintain its original dimensions but with the advantages of FBG. The optical fiber cable, or the 250 μm optical fiber with its protection sleeve, had an outside diameter of 3 mm. For most purposes, all sensors placed inside the triaxial cell can share a common optical fiber cable because of the distributive capabilities of the FBG sensors. If necessary, optical fiber housed in a 0.9 mm plastic tubing can be used to replace the 3 mm cable. These unique features help alleviate congestion within the triaxial cell. A qualitative cost comparison between the FBG and electric sensor systems is shown in Table 2. In most cases, due to relatively simple mechanisms, the FBG sensors should have lower costs than their electric counterparts. The FBG data logger is many times more expensive than the commercially available digital data logging systems for electric sensors. Unlike the electric sensors, however, the FBG does not require signal conditioning and thus can offer some cost advantage for FBG systems.

The FBG pressure transducers in their current designs need independent measurement for compensating temperature effects. The temperature compensation for the load cell and displacement transducer has been dealt with by using paired FBGs where one FBG experiences tension and the other compression when the sensor is loaded. The temperature effects that cause both FBGs to experience tension or compression simultaneously are eliminated when one reading is subtracted from the other. Similar technique can be used for the pressure transducers. However, this would require that two FBGs be placed at 10 mm apart on the same optical fiber so that both FBGs can be fitted inside of the pressure transducer, and one on each side of the diaphragm (see Fig. 8). This type of FBG pairs will have to be specially ordered and the cost is high without quantity.

TABLE 2—Comparison of cost between the FBG and electric sensor systems.

Sensor	Cost Difference between FBG and Electric Sensors ^a
Submersible displacement transducer	$\pm 30\%$
Submersible load cell	-50 to +10 %
Gauge pressure transducer	$\pm 30\%$
Differential pressure transducer	-50 to +10 %
Signal condition and data logger	+200 % and above

^aCost difference=(cost of FBG sensor - cost of electric sensor) $\times 100\%/(cost\ of\ electric\ sensor)$.

The FBG sensors described in the paper are laboratory built, prototype units. The calibration of FBG sensors showed significant hysteresis in most cases (i.e., in Figs. 4, 7, 9, and 10). Better mechanical design and/or material treatment would be desirable for streamlining the performance of the FBG sensors. With the minute dimensions and other superior features of FBGs, such improvement should not be an insurmountable task. The cost of FBG has become affordable recently as the demand increases. As the cost of data acquisition unit continues to decrease, it is conceivable that the FBG sensors can become a viable choice for laboratory geotechnical testing as it has been the case for field monitoring.

Concluding Remarks

The authors experimented with the use of fiber optic sensors for displacement, force, and pressure measurements in a series of triaxial tests involving saturated and unsaturated soil specimens. The FBG sensors are partially distributive and passive in nature, and they are immune to short circuit and EMI even when submerged under water. These unique features make FBG sensors easy to setup for triaxial testing. Available test results showed promising performances when compared with reference readings from conventional means.

Acknowledgments

Research described in the paper was funded by the National Science Council of Taiwan under Contract No. 97-2625-M-009-009. The support is gratefully acknowledged.

References

Agrawal, G. P., 2002, *Fiber-Optic Communication Systems*, 3rd ed., Wiley-Interscience, New York.

Burland, J. B., 1989, "Small is Beautiful-the Stiffness of Soil at Small Strain," *Can. Geotech. J.*, Vol. 26(4), pp. 499–516.

Fredlund, D. G. and Rahardjo, H., 1993, *Soil Mechanics for Unsaturated Soils*, John Wiley & Sons, Inc., New York.

Goto, S., Tatsuoka, F., Shibuya, S., Kim, Y. S., and Sato, T., 1991, "A Simple Gauge for Local Small Strain Measurements in the Laboratory," *Soils Found.*, Vol. 31(1), pp. 169–180.

Hill, K. O., Fujii, Y., Johnson, D. C., and Kawasaki, B. S., 1978, "Photosensitivity in Optical Fiber Waveguides: Application to Reflection Filter Fabrication," *Appl. Phys. Lett.*, Vol. 32, pp. 647–649.

Ho, Y. T., Huang, A. B., and Lee, J. T., 2006, "Development of a Fiber Bragg Grating Sensed Ground Movement Monitoring System," *Meas. Sci. Technol.*, Vol. 16, pp. 1733–1740.

Ho, Y. T., Huang, A. B., and Lee, J. T., 2008, "Development of a Chirped/Differential Optical Fiber Bragg Gating Pressure Sensor," *Meas. Sci. Technol.*, Vol. 19, 045304.

Huang, A. B. and Hsu, H. H., 2005, "Cone Penetration Tests under Simulated Field Conditions," *Geotechnique*, Vol. 55(5), pp. 345–354.

Kersey, A. D., 1992, "Multiplexed Fiber Optic Sensors," *Proceedings, Fiber Optic Sensors*, E. Udd, Ed., Boston, Massachusetts, 8–11 Sept. 1992, SPIE-The International Society for Optical Engineering, Bellingham, Washington, pp. 200–227.

Meltz, G., Morey, W. W., and Glam, W. H., 1989, "Formation of Bragg Grating in Optical Fibers by Transverse Holographic Method," *Opt. Lett.*, Vol. 14, pp. 823–825.

Ng, C. W. W., Zhan, L. T., and Cui, Y. J., 2002, "A New Simple System for Measuring Volume Changes in Unsaturated Soils," *Can. Geotech. J.*, Vol. 39, pp. 757–764.

Rao, Y.-J., 1998, *Optic Fiber Sensor Technology*, K. T. V. Gattan and B. T. Meggitt, Eds., Chapman and Hall, London, Vol. 2, pp. 355–379.

Timoshenko, S. P. and Woinowsky-Krieger, S., 1959, *Theory of Plates and Shells*, 2nd ed., McGraw-Hill, New York.